Published in "Physical Review Letters 104: 156807, 2010"
which should be cited to refer to this work.

Dynamical Response and Confinement of the Electrons at the $LaAlO_3/SrTiO_3$ Interface

A. Dubroka,[1] M. Rössle,[1] K. W. Kim,[1] V. K. Malik,[1] L. Schultz,[1] S. Thiel,[2] C. W. Schneider,[2,3] J. Mannhart,[2] G. Herranz,[4,*] O. Copie,[4] M. Bibes,[4] A. Barthélémy,[4] and C. Bernhard[1,†]

[1]*University of Fribourg, Department of Physics and Fribourg Center for Nanomaterials, Chemin du Musée 3, CH-1700 Fribourg, Switzerland*

[2]*Experimental Physics VI, Center for Electronic Correlations and Magnetism, Institute of Physics, University of Augsburg, D-86135 Augsburg, Germany*

[3]*Paul Scherrer Institut, Materials Group, 5232, Villigen, Switzerland*

[4]*Unité Mixte de Physique CNRS/Thales associée à l'Université Paris-Sud, Campus de l'Ecole Polytechnique, 1 Avenue A. Fresnel, 91767 Palaiseau, France*

With infrared ellipsometry and transport measurements we investigated the electrons at the interface between $LaAlO_3$ and $SrTiO_3$. We obtained a sheet carrier concentration of $N_s \approx 5$–9×10^{13} cm^{-2}, an effective mass of $m^* = 3.2 \pm 0.4 m_e$, and a strongly frequency dependent mobility. The latter are similar as in bulk $SrTi_{1-x}Nb_xO_3$ and therefore suggestive of polaronic correlations. We also determined the vertical concentration profile which has a strongly asymmetric shape with a rapid initial decay over the first 2 nm and a pronounced tail that extends to about 11 nm.

PACS numbers: 73.40.−c, 73.50.Mx, 78.30.−j

It has been demonstrated that highly mobile charge carriers can develop at the interface between a $SrTiO_3$ (STO) substrate and a thin $LaAlO_3$ (LAO) layer that is grown on top [1–10]. This came as a surprise since both materials are insulators with $\Delta_{gap}^{STO} = 3.2$ eV and $\Delta_{gap}^{LAO} = 5.6$ eV, respectively. These carriers have been suggested to originate from an electronic reconstruction across the heteropolar interface which gives rise to a transfer of $1/2e$ charge per unit cell yielding a sheet carrier concentration of $N_s = 3.3 \times 10^{14}$ cm^{-2}. Supporting this so-called polarization catastrophe scenario, transport measurements showed that a critical thickness of 4 LAO unit cells and thus a minimal electrostatic potential is required for the conducting layer to develop [3], albeit the N_s measured by the Hall effect is only 2–6 $\times 10^{13}$ cm^{-2}. It has also been argued that the carriers are induced via oxygen vacancies [5] or interfacial mixing of La and Sr [11]. While this question remains unsettled, it was shown that the carrier concentration can be largely varied by applying a gate voltage, thus allowing for a reproducible switching between insulating, metallic, and even superconducting states [3,12]. These exciting developments inspired large theoretical efforts [13,14] and raised hopes that these oxides may be useful for new electronic devices [15] and for studying electric field induced quantum phase transitions. Accordingly, the fundamental properties of these confined charge carriers are a subject of utmost importance.

In this letter we present infrared (IR) ellipsometry data which provide such information. In the first part (Figs. 1 and 2), we combine far-infrared (FIR) and transport data to obtain the effective mass. In the second part (Fig. 3), we analyze a Berreman mode which yields direct information about the depth profile of the carrier concentration.

The LAO-STO heterostructures were grown by pulsed laser deposition. Two samples were grown in Augsburg at O_2 pressure of 6×10^{-5} mbar. They were subsequently annealed to remove any oxygen vacancies in the STO substrate which could induce bulk metallicity [6]. The LAO layer thickness of 3 and 5 unit cells (LS-3 and LS-5) was chosen to lie below and above the critical value where a conducting interface layer develops [3]. Samples LS-50 and LS-50-ov were grown in Palaiseau at O_2 pressures of 10^{-4} and 10^{-6} mbar [4] to render the STO substrate insulating and conducting, respectively [6].

Ellipsometry enables accurate and direct measurements of the real and imaginary parts of the pseudodielectric function, ϵ_1 and ϵ_2. The measurements between 100–5000 cm^{-1} were performed with a homebuilt setup attached to a Bruker 113V fast-Fourier spectrometer [16]. The angle of incidence of the light was 75°; a ZnSe compensator was used above 700 cm^{-1}. Photodoping [17] was avoided by shielding the sample against visible and UV light.

Figure 1 shows the FIR data which reveal the Drude response of the mobile electrons at the LAO-STO interface. Figure 1(a) compares the spectra of ϵ_1 and ϵ_2 for LS-5 and bare STO. They almost coincide and are dominated by the STO phonons near 545, 175 and the strong so-called soft mode below 100 cm^{-1}. Nevertheless, as shown in the insets, some small, yet significant differences appear upon magnification. Figure 1(b) shows the corresponding difference spectra of $\Delta\epsilon_{1,2} = \epsilon_{1,2}(\text{LS-5}) - \epsilon_{1,2}(\text{STO})$. Here the inductive response of the charge carriers is evident from the temperature (T) and frequency dependent decrease of $\Delta\epsilon_1$ (upper panel). The data are well reproduced (middle and bottom panel) with a model (solid lines) that contains a conducting layer at the LAO-STO interface with a rectan-

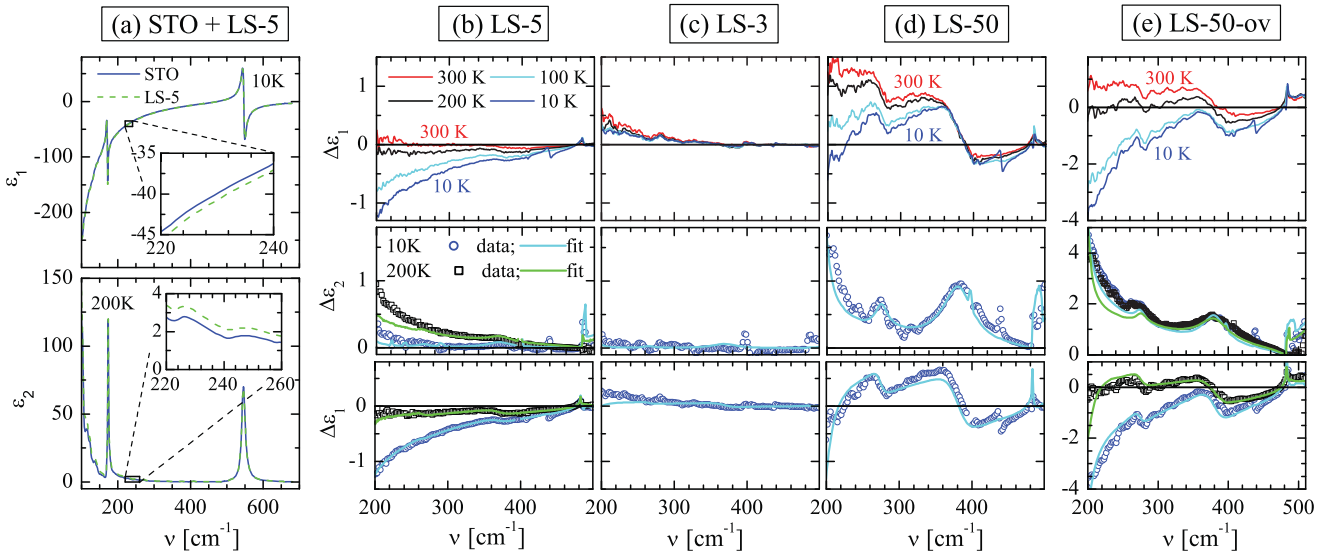

FIG. 1 (color). (a) Spectra of ϵ_1 (10 K) and ϵ_2 (200 K) for LS-5 (dashed lines) and bare $SrTiO_3$ (solid lines). Insets: Magnification of the differences. Corresponding spectra of $\Delta\epsilon_{1,2} = \epsilon_{1,2} - \epsilon_{1,2}(\mathrm{STO})$ for LS-5 (b), LS-3 (c), LS-50 (d), and LS-50-ov (e) showing the Drude response. Top panels show the T dependence of $\Delta\epsilon_1$. Middle and bottom panels show $\Delta\epsilon_1$ and $\Delta\epsilon_2$ as obtained from experiment (symbols) and model calculations (lines), respectively.

gular concentration profile and a thickness d that is much smaller than the penetration depth of the IR light, $p_{\mathrm{IR}} \approx 1\ \mu$m; for details see Ref. [18]. Figures 1(c) and 1(d) show the data on LS-3 and LS-50 which confirm that we are probing the Drude response of interfacial charge carriers. For LS-3 there is no clear indication of an inductive decrease of $\Delta\epsilon_1$, while for LS-50 the magnitude of the inductive response is similar as in LS-5. These trends agree with a previous report that the conducting layer develops only above a LAO thickness of 4 unit cells [3]. Finally, Fig. 1(e) shows our data for LS-50-ov where even the bulk of the STO substrate is known to be conducting [7]. Accordingly, its inductive response is significantly stronger than in LS-50 and LS-5 (note the enlarged vertical scale).

The results of a quantitative analysis and the comparison with the transport (TR) data are detailed in Fig. 2. The Drude response is well approximated by the volumetric average of ϵ of the individual layers since $\lambda_{\mathrm{IR}} \gg p_{\mathrm{IR}} \gg d$, where λ_{IR} is the wavelength. The measured strength of the Drude response is thus proportional to $d\omega_{\mathrm{pl}}^2 = N_s^{\mathrm{IR}} e^2/\epsilon_0 m^*$, where ω_{pl}, m^*, e, and ϵ_0 are the plasma frequency, effective carrier mass, electric charge, and dielectric constant, respectively. N_s^{IR} is the sheet carrier concentration probed upon reflection of the IR radiation. Furthermore, we obtain the scattering rate γ or the electron mobility $\mu^{\mathrm{IR}} = e/(m^* 2\pi c\gamma)$. In addition, m^* can be deduced under the condition that the IR and transport measurements are probing the same laterally homogeneous electron system and thus yield the same values for N_s^{IR} and N_s^{TR}, respectively. Figures 2(a) and 2(b) show N_s and μ of LS-5 obtained by transport (open squares) and calculated from IR data (solid circles) with $m^* = 3.2 \pm 0.4 m_e$. The latter was obtained by matching $N_s^{\mathrm{IR}} = N_s^{\mathrm{TR}}$ for $T \geq 100$ K and is used in our further analysis. Notably, the value of m^* is similar to the one of bulk $SrTi_{1-x}Nb_xO_3$ [19] where the electrons reveal polaronic correlations. In the latter m^* gradually decreases at low T. The increase of N_s^{IR} at 10 K thus may be the signature of a corresponding decrease of m^*. The sudden decrease of N_s^{TR} below 100 K likely has a different origin, possibly due to a weak localization which affects the dc response but hardly the IR one. The reason might be a tilting of the STO substrate below a structural transition which has been observed on another oxide heterostructure [20].

In comparing the different samples, we find that LS-5 and LS-50 (see also Fig. 2) have similar values of $N_s^{\mathrm{IR}} \approx 9 \times 10^{13}$ cm^{-2} at 10 K. This is despite a tenfold difference in the LAO layer thickness and the fact that the samples were grown in different conditions and growth chambers. A significantly enhanced Drude response is only observed in LS-50-ov where it is well established that additional

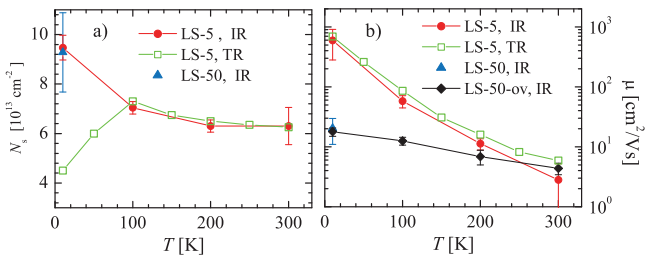

FIG. 2 (color). Comparison of the sheet carrier concentration N_s (a) and mobility μ (b) as deduced from IR (full symbols) and transport (TR, open symbols) measurements. The values deduced from the IR data were calculated using $m^* = 3.2 m_e$ as discussed in the text. Error bars represent 1 standard deviation.

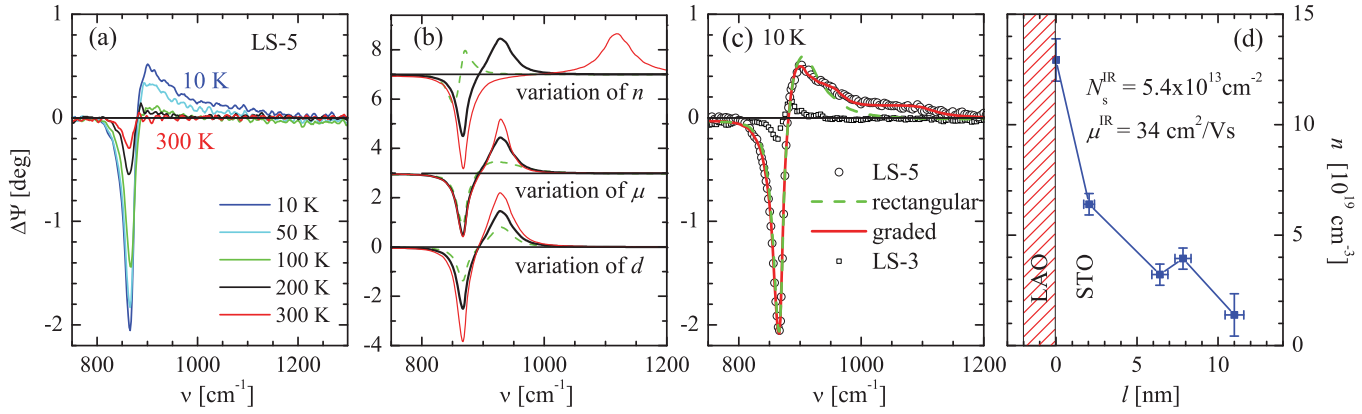

FIG. 3 (color). (a) Difference spectra of the ellipsometric angle, $\Delta\Psi = \Psi(\text{LS-5}) - \Psi(\text{STO})$, showing the Berreman mode in the vicinity of the highest LO phonon of STO. (b) Simulations of $\Delta\Psi$ with a rectangular concentration profile of the conducting layer. Shown from top to bottom (shifted for clarity) are the changes with respect to the thick solid line ($d = 11$ nm, $n = 5 \times 10^{13}$ cm^{-3}, $\mu = 33$ cm^2/V s) upon variation of n (dashed, 2.2×10^{13} cm^{-3}, thin solid 13×10^{13} cm^{-3}), of μ (dashed 10 cm^2/V s, thin solid 80 cm^2/V s), and d (dashed 6 nm, thin solid 17 nm). (c) Comparison between the data of LS-5 at 10 K (circles) and calculations assuming a rectangular (dashed line) and a graded profile (solid lines) of the conducting layer. The corresponding data for LS-3 are shown as squares. (d) Depth profile of n as obtained from the fit (solid line) in (c). Error bars represent 1 standard deviation.

charge carriers caused by oxygen vacancies are present in the bulk of the STO substrate [4,7]. In agreement with this conjecture, we find that the value of $N_s^{\text{TR}} = 1 \times 10^{16}$ cm^{-2} is significantly higher than $N_s^{\text{IR}} = 4 \times 10^{14}$ cm^{-2} since the latter is limited by the probe depth of the IR light of $p_{\text{IR}} \approx 1$ μm. The difference in probe depth can also explain the discrepancy between the low-T values of $\mu^{\text{IR}} \approx 20$ cm^2/V s and $\mu^{\text{TR}} \approx 10^4$ cm^2/V s of LS-50-ov [4] if the carriers near the interface are more strongly scattered on defects than the ones in the bulk.

Next we present the analysis of a Berreman mode [21] which provides insight into the vertical concentration profile of the mobile carriers [22,23]. Berreman modes arise from a dynamical charge accumulation at interfaces of heterostructures that is driven by the normal component of the polarized light. Accordingly, they give rise to IR-active dipoles and corresponding resonances near the longitudinal optical (LO) modes of the constituent materials [24]. These features show up in the reflection coefficient r_p for parallel (p) polarization with respect to the plane of incidence and are absent in the coefficient r_s for perpendicular (s) polarization. Accordingly, as shown in Fig. 3, the signatures of a Berreman mode are well represented in terms of the ellipsometric angle $\Psi = \arctan(|r_p/r_s|)$. Figure 3(a) shows the T dependence of the difference spectrum $\Delta\Psi$ between LS-5 and bare STO. It contains a feature with a sharp minimum around 865 cm^{-1} and a broader maximum near 900 cm^{-1} that becomes pronounced at low T. The latter corresponds to the structure in r_p near ω_{LO} of the conducting layer. The former arises from the polarization dependence of the reflection coefficient near $\epsilon_1 = 1$. Figure 3(b) displays simulations which show that these features in $\Delta\Psi$ undergo characteristic changes as a function of n, μ, and d. For the minimum, these parameters mostly affect the magnitude but hardly the shape and position. For the maximum, the center frequency strongly increases as a function of n while it hardly changes with μ and d. The upward shift of the maximum with respect to $\omega_{\text{LO}} = 788$ cm^{-1} in bare STO thus provides a direct measure of n. A distinction between μ and d is also possible since the former (latter) gives rise to an asymmetric (symmetric) change in the intensity of the maximum and minimum, respectively. The result of our analysis is summarized in Fig. 3(c) which displays the data at 10 K together with the best fits using two different models. The dashed line shows the case of a rectangular profile of the electron concentration on the STO side of the LAO-STO interface which yields $N_s = 5 \times 10^{13}$ cm^{-2}, $d = 12$ nm, and $\mu = 10$ cm^2/V s. While this model does not fully account for the spectra, it provides a first indication that the electronic charge is spread over a significant range of at least 10 nm. The differences with respect to the data, in particular, the missing tail towards higher frequency are a clear indication that n exhibits a sizable variation in the normal direction. As shown by the solid line, an excellent agreement is obtained with a model that allows for a depth variation of n. The obtained concentration profile is displayed in Fig. 3(d). We have assumed that the profile consists of 4 sublayers where the concentration varies linearly and that n is maximal at the LAO-STO interface. The concentration at the boundaries between the sublayers and their depth position was obtained by a least square fit to the data. The stability of the fitting procedure is outlined in Ref. [18]. The profile has a sharp maximum at the interface with a carrier concentration of 1.3×10^{20} cm^{-3} and a full width at half maximum of only 2 nm. In addition, it has a pronounced tail that extends to 11 ± 0.6 nm and contains about 2/3 of the total $N_s^{\text{IR}} = 5.4 \times 10^{13}$ cm^{-2} (assuming $m^* = 3.2 m_e$). The obtained mobility amounts to $\mu^{\text{IR}} = 34$ cm^2/V s. Notably, the former value agrees well with the one as derived from the Drude response. This is especially true since additional

weight may be contained in an extension of the tail beyond 11 nm that is below the resolution at this frequency range. Irrespective of this uncertainty, our transport and IR data (assuming here $m^* \sim 3m_e$ [19]) consistently yield a value of $N_s \approx 5$–9×10^{13} cm^{-2} that is several times smaller than the prediction of $N_s = 3.3 \times 10^{14}$ cm^{-2} of the polarization catastrophe scenario. Unless our interpretation is not correct and $m^* \geq 10m_e$ at FIR frequencies, this implies that the majority of the electrons are localized with a binding energy E_b in excess of 0.1 eV. Finally, we mention that only a tiny signature of the Berreman mode could be observed in LS-3 [see Fig. 3(c)]. In LS-50 and LS-50-ov the mode is lacking a well resolved maximum (not shown) in agreement with the much lower μ values as derived from the Drude response.

The obtained charge concentration profile can be well reconciled with previous reports. It is consistent with the observation of superconductivity since the distribution of n matches the region of the maximum of the superconducting dome of bulk STO [25]. It agrees with a corresponding estimate of $d < 10$ nm [8] and also with a scaling analysis of the anisotropy of the upper critical field which yields $\approx$ 7 nm [26]. The strongly asymmetric profile also confirms the calculations in Ref. [27] which take into account the large local electric field and the strongly nonlinear polarizibility of STO at the interface. Our full width at half maximum of 2 nm is, however, smaller than the reported experimental value of 12 nm at 10 K [27]. Our profile also seems consistent with the claim of Ref. [28] that the carrier concentration decreases very rapidly within the first 4 nm, albeit their measurements were performed at 300 K where the profile is reported to be narrower [27]. In this comparison one should consider that different definitions of d were used and that the various techniques are either more sensitive to the high concentration at the interface or rather to the long tail which contains most of the weight. In this context we emphasize the significance of our optical data which provide a truly macroscopic (in the lateral direction) and fairly direct probe of the concentration profile.

Finally, we comment on the marked difference between $\mu^{\mathrm{IR}} = 34$ cm^2/V s as derived from the Berreman mode at 900 cm^{-1} and the corresponding $\mu^{\mathrm{IR}} = 700$ cm^2/V s from the Drude response at low frequency. Notably, a similar frequency dependence of the mobility, or a strong inelastic contribution to the scattering rate, was observed in bulk $SrTi_{1-x}Nb_xO_3$ [19] and explained in terms of polaronic correlations.

In summary, with IR ellipsometry and transport measurements we determined the sheet carrier concentration of $N_s \approx 5$–9×10^{13} cm^{-2} of the electrons at the LAO-STO interface and showed that the additional electrons expected within the electronic reconstruction scenario must be strongly bound with $E_b \geq 0.1$ eV. We deduced an effective mass of $m^* = 3.2 \pm 0.4m_e$ and a strongly frequency dependent mobility which are similar as in bulk $SrTi_{1-x}Nb_xO_3$ and thus suggestive of polaronic correlations of the confined electrons. We also determined the vertical profile of the carrier concentration which is strongly asymmetric with an initial fast decay over 2 nm followed by a pronounced tail that extends to about 11 nm.

We appreciate discussions with J. Humlíček and A. J. Millis and technical support by Y.-L. Mathis at the ANKA synchrotron at FZ Karlsruhe, where parts of the work were performed. We acknowledge financial support in Fribourg by the SNF (Grants No. 200020-119784, No. 200020-129484, and NCCR-MaNEP), in Augsburg by the DFG (TRR80, SFB484) and the EC (Nanoxide, OxIDes), and at Unité Mixte de Physique CNRS by the French ANR program "Oxitronics."

*Institut de Ciència de Materials de Barcelona, ICMAB-CSIC Campus de la UAB, Bellaterra 08193, Spain.
†christian.bernhard@unifr.ch

[1] A. Ohtomo and H. Y. Hwang, Nature (London) **427**, 423 (2004).
[2] N. Nakagawa, H. Y. Hwang, and D. A. Muller, Nature Mater. **5**, 204 (2006).
[3] S. Thiel *et al.*, Science **313**, 1942 (2006).
[4] G. Herranz *et al.*, Phys. Rev. Lett. **98**, 216803 (2007).
[5] A. Kalabukhov *et al.*, Phys. Rev. B **75**, 121404(R) (2007).
[6] W. Siemons *et al.*, Phys. Rev. Lett. **98**, 196802 (2007).
[7] M. Basletic *et al.*, Nature Mater. **7**, 621 (2008).
[8] N. Reyren *et al.*, Science **317**, 1196 (2007).
[9] A. Brinkman *et al.*, Nature Mater. **6**, 493 (2007).
[10] M. Breitschaft *et al.*, arXiv:0907.1176.
[11] P. R. Willmott *et al.*, Phys. Rev. Lett. **99**, 155502 (2007).
[12] A. D. Caviglia *et al.*, Nature (London) **456**, 624 (2008).
[13] K. Janicka, J. P. Velev, and E. Y. Tsymbal, Phys. Rev. Lett. **102**, 106803 (2009).
[14] R. Pentcheva and W. E. Pickett, Phys. Rev. Lett. **102**, 107602 (2009).
[15] C. Cen *et al.*, Science **323**, 1026 (2009).
[16] C. Bernhard, J. Humlíček, and B. Keimer, Thin Solid Films **455–456**, 143 (2004).
[17] Y. Kozuka, Y. Hikita, T. Susaki, and H. Y. Hwang, Phys. Rev. B **76**, 085129 (2007).
[18] See supplementary material at http://link.aps.org/supplemental/10.1103/PhysRevLett.104.156807 for specific details of the data analysis.
[19] J. L. M. van Mechelen *et al.*, Phys. Rev. Lett. **100**, 226403 (2008).
[20] J. Hoppler *et al.*, Phys. Rev. B **78**, 134111 (2008).
[21] D. W. Berreman, Phys. Rev. **130**, 2193 (1963).
[22] J. Humlíček, R. Henn, and M. Cardona, Appl. Phys. Lett. **69**, 2581 (1996).
[23] M. Schubert, *Infrared Ellipsometry on Semiconductor Layer Structures* (Springer, Heidelberg, 2004).
[24] A. Sihvola, *Electromagnetic Mixing Formulas and Applications* (The Institution of Electrical Engineers, London, 1999).
[25] C. S. Koonce *et al.*, Phys. Rev. **163**, 380 (1967).
[26] T. Schneider, Phys. Rev. B **80**, 214507 (2009).
[27] O. Copie *et al.*, Phys. Rev. Lett. **102**, 216804 (2009).
[28] M. Sing *et al.*, Phys. Rev. Lett. **102**, 176805 (2009).